GEOLOGY

A nearly water-saturated mantle transition zone inferred from mineral viscosity

Hongzhan Fei,[1,2]* Daisuke Yamazaki,[1] Moe Sakurai,[1,3] Nobuyoshi Miyajima,[2] Hiroaki Ohfuji,[4] Tomoo Katsura,[2] Takafumi Yamamoto[5]

An open question for solid-earth scientists is the amount of water in Earth's interior. The uppermost mantle and lower mantle contain little water because their dominant minerals, olivine and bridgmanite, have limited water storage capacity. In contrast, the mantle transition zone (MTZ) at a depth of 410 to 660 km is considered to be a potential water reservoir because its dominant minerals, wadsleyite and ringwoodite, can contain large amounts of water [up to 3 weight % (wt %)]. However, the actual amount of water in the MTZ is unknown. Given that water incorporated into mantle minerals can lower their viscosity, we evaluate the water content of the MTZ by measuring dislocation mobility, a property that is inversely proportional to viscosity, as a function of temperature and water content in ringwoodite and bridgmanite. We find that dislocation mobility in bridgmanite is faster by two orders of magnitude than in anhydrous ringwoodite but 1.5 orders of magnitude slower than in water-saturated ringwoodite. To fit the observed mantle viscosity profiles, ringwoodite in the MTZ should contain 1 to 2 wt % water. The MTZ should thus be nearly water-saturated globally.

INTRODUCTION

Unlike the dry uppermost mantle and lower mantle, Earth's mantle transition zone (MTZ) at a depth of 410 to 660 km is a potential water reservoir (*1*, *2*), but the exact water content of the MTZ is a matter of debate. A ringwoodite inclusion with 1.4 weight % (wt %) water was recently found in a diamond crystal from kimberlite in Brazil, which suggests a water-rich MTZ (*3*). However, this inclusion might only reflect local conditions because kimberlite magma is generally rich in volatile components, such as water and CO_2 (*4*). Furthermore, these kimberlite eruptions occur in a few places and do not reflect mantle characteristics globally (*5*). Significant effort has been expended to estimate the water content of the MTZ based on electrical conductivity, but various research groups have estimated markedly different values (*6*–*9*). Their results differ by more than one order of magnitude, which is likely because of the difficulty of performing laboratory conductivity experiments and modeling the magnetotelluric observations. Seismic observations and melting experiments suggest a water-rich MTZ (*10*), but quantitatively assessing the water content based on this approach is impossible because no firm numerical relationship has been identified between water content and seismic velocity. Thus, we currently have no definite knowledge about the water content of the MTZ.

Because incorporation of water can lower the viscosity of nominally anhydrous minerals (*11*), it should be possible to evaluate the water content of the MTZ by comparing results from laboratory rheological data for the dominant MTZ minerals with mantle viscosities inferred from postglacial rebound and gravity data (*12*–*14*). A prominent characteristic of mantle viscosity derived from the postglacial rebound data is that it increases by more than an order of magnitude from the MTZ to the lower mantle. Therefore, we can estimate the water content of the MTZ by comparing the viscosities of ringwoodite and bridgmanite, which are the dominant minerals in the lower part of MTZ and lower mantle, respectively.

Currently, the typical approach to investigating mineral viscosity involves deformation experiments using a deformation multianvil apparatus (D-DIA) or a rotational Drickamer apparatus (*15*, *16*). However, the stresses in these experiments are many orders of magnitude higher than those in Earth's mantle, and the stress-strain rate relationships may differ under high- and low-stress conditions (*17*). This variation could lead to a misinterpretation of the conditions in Earth's interior.

An alternative method for investigating mineral viscosity is to conduct dislocation recovery experiments. As we know, the plastic deformation of rocks and minerals in Earth's interior is controlled by either dislocation creep or diffusion creep, which are driven by the motion of dislocations and point defects within crystalline materials, respectively. Dislocation creep produces seismic anisotropy, whereas diffusion creep does not. In the MTZ, the results of Si diffusion experiments and observations of seismic anisotropy suggest that dislocation creep dominates (*18*–*20*). In the lower mantle, although most regions are seismically isotropic (*19*, *21*), the straight shapes of mantle plumes indicate that horizontal flow does not occur (*19*); therefore, dislocation creep is not ruled out. In addition, the uppermost regions of the lower mantle from 660 to approximately 1000 km in depth do show some anisotropy (*19*, *22*), suggesting that dislocation creep is present. Thus, dislocation creep probably operates in at least these regions of the lower mantle. Under high-temperature and low-stress conditions, such as those in Earth's interior, dislocation creep involves dislocation climb and dislocation glide processes in the crystals (*23*–*25*), both of which are controlled by dislocation motion. Therefore, the viscosity of ringwoodite and bridgmanite under the conditions of the MTZ and lower mantle can be investigated by measuring their dislocation mobilities within their crystal structures.

Here, we measured the dislocation mobility as a function of temperature and water content in ringwoodite at 22 GPa and as a function of temperature in bridgmanite at 25 GPa. On the basis of assumptions of the dominance of dislocation creep and the linear relationship between the creep rate and dislocation mobility described by the Orowan equation, we obtained the difference in viscosity between the MTZ and the lower mantle from the dislocation mobility difference between ringwoodite and bridgmanite.

[1]Institute for Study of the Earth's Interior, Okayama University, Misasa, Tottori 682-0193, Japan. [2]Bayerisches Geoinstitut, Universität Bayreuth, Bayreuth D95440, Germany. [3]Department of Earth and Planetary Sciences, Tokyo Institute of Technology, Tokyo 152-8551, Japan. [4]Geodynamics Research Center, Ehime University, Matsuyama 790-8577, Japan. [5]Department of Earth and Planetary Systems Science, Hiroshima University, Hiroshima 739-8526, Japan.
*Corresponding author. Email: hongzhan.fei@uni-bayreuth.de

With these results, we demonstrated that the MTZ contains 1 to 2 wt % water globally.

RESULTS AND DISCUSSION

We nucleated dislocations in synthetic ringwoodite and bridgmanite samples by applying stresses to the samples under high-pressure and high-temperature conditions. Through the subsequent annealing of samples under quasi-hydrostatic conditions, dislocations with opposite signs coalesced and annihilated, causing the dislocation density to decrease (Fig. 1). This dislocation annihilation was expected to be rate-limited by climb, although the annihilation involves both climb and glide processes (*23*–*25*).

The dislocation annihilation rate (k) could be calculated from the dislocation densities before (ρ_i) and after (ρ_f) annealing over annealing time (t) using the equation (*26*) as follows

$$k = \left(\frac{1}{\rho_f} - \frac{1}{\rho_i}\right)/t \quad (1)$$

Because dislocation mobility is proportional to the annihilation rate (*26*), we used the dislocation annihilation rate as a proxy for the mobility to define the difference in viscosity between ringwoodite and bridgmanite. Figure 2 shows that the dislocation mobility proxied by annihilation rate systematically increased with increasing temperature in both ringwoodite and bridgmanite. In ringwoodite, it increased with water content. We fit the data points to Arrhenius equations for ringwoodite (rw.) and bridgmanite (brg.) as follows

$$k(\text{rw.}) = k_{0,\text{rw.}}(C_{\text{H20}})^r \exp\left(-\frac{\Delta H_{\text{rw.}}}{RT}\right) \quad (2)$$

$$k(\text{brg.}) = k_{0,\text{brg.}} \exp\left(-\frac{\Delta H_{\text{brg.}}}{RT}\right) \quad (3)$$

where C_{H2O} is the water content in parts per million by weight (wt ppm), r is the water content exponent, R is the ideal gas constant, T is the absolute temperature, $k_{0,\text{rw.}}$ and $k_{0,\text{brg.}}$ are the pre-exponential factors, $\Delta H_{\text{rw.}}$ and $\Delta H_{\text{brg.}}$ are the activation enthalpies, and k(rw.) and

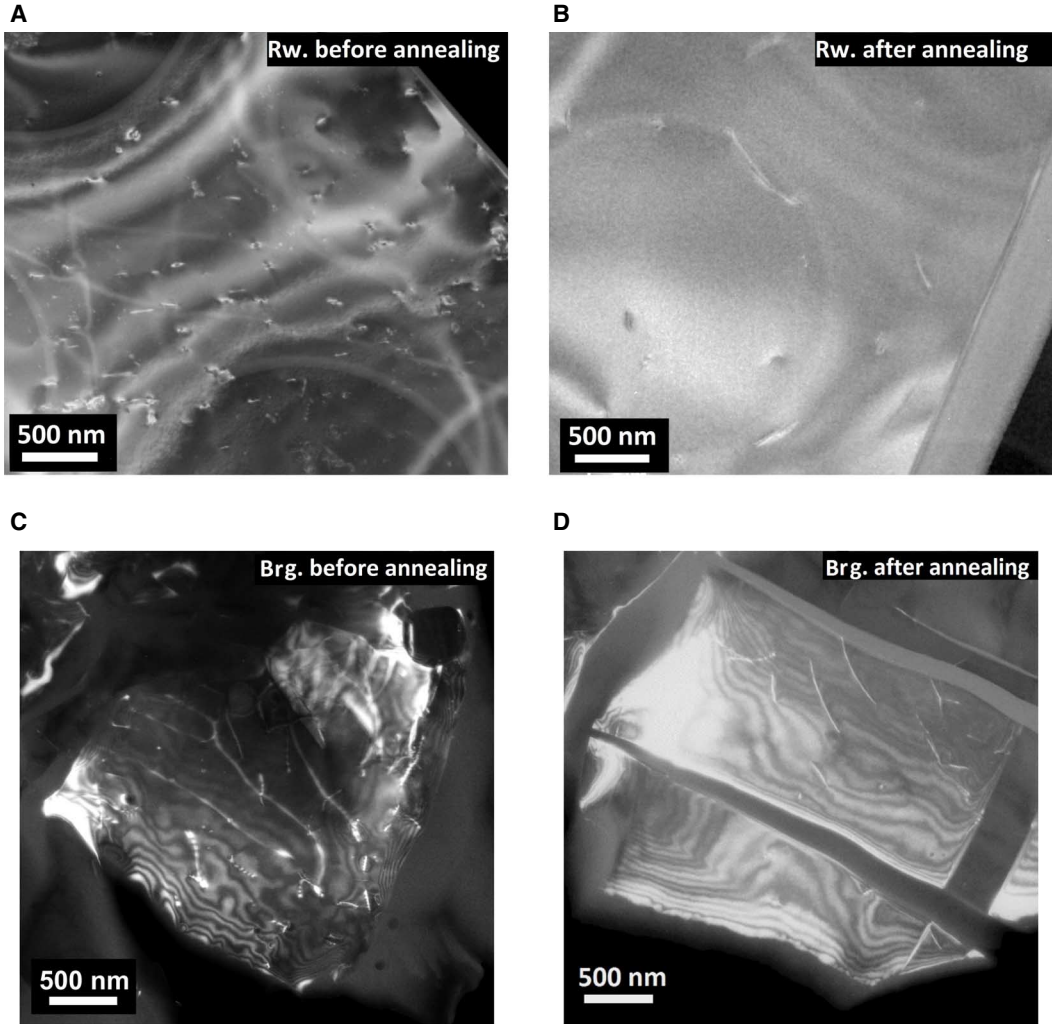

Fig. 1. TEM images of ringwoodite and bridgmanite before and after annealing. (**A**) Inverted bright-field image of ringwoodite before annealing ($\rho_i = 11.0/\mu m^2$). (**B**) Inverted bright-field image of ringwoodite after annealing for 12 hours at 2000 K ($\rho_f = 0.87/\mu m^2$). (**C**) Dark-field image of bridgmanite before annealing ($\rho_i = 8.43/\mu m^2$). (**D**) Dark-field image of bridgmanite after annealing for 24 hours at 1600 K ($\rho_f = 4.32/\mu m^2$). Rw., ringwoodite; Brg., bridgmanite.

k(brg.) are the dislocation mobilities in ringwoodite and bridgmanite, respectively. We found that $k_{0,rw.} = 10^{-11.6\pm0.8}$ m^2/s, $r = 1.1 \pm 0.1$, $\Delta H_{rw.} = 300 \pm 30$ kJ/mol, $k_{0,brg.} = 10^{-6.8\pm1.1}$ m^2/s, and $\Delta H_{brg.} = 330 \pm 40$ kJ/mol.

The dislocation motion in crystals at high temperatures is related to self-diffusion of elements. The activation enthalpy for dislocation motion in ringwoodite is much smaller than that for Si self-diffusion (480 ± 90 kJ/mol) but close to that for O diffusion (370 ± 80 kJ/mol) within experimental uncertainties (*20*). Thus, the dislocation motion in ringwoodite may be controlled primarily by O diffusion. In bridgmanite, both Si and Mg are the slowest diffusing species, with activation enthalpies of about 310 to 410 kJ/mol (*27*, *28*), which are close to the value determined for bridgmanite in this study. Therefore, dislocation motion in bridgmanite is probably controlled by either Si or Mg diffusion.

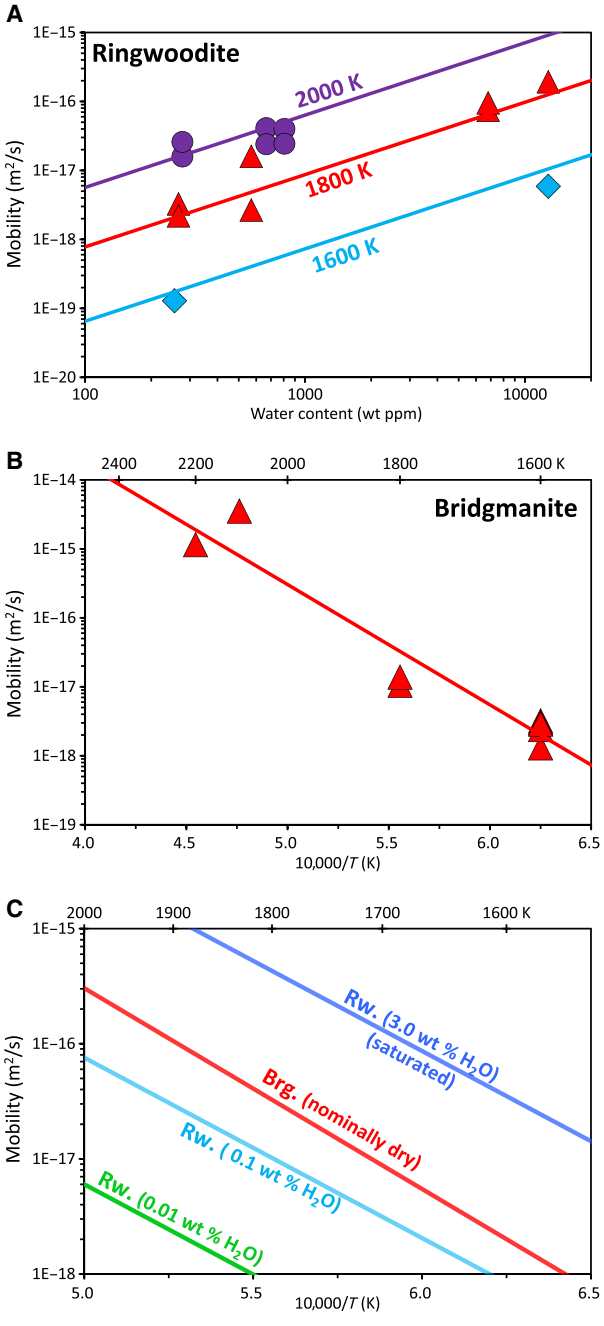

Fig. 2. Results of dislocation recovery experiments on ringwoodite and bridgmanite. (**A**) Dislocation mobility in ringwoodite as a function of water content at different temperatures. (**B**) Dislocation mobility in bridgmanite as a function of temperature. (**C**) Comparison of dislocation mobilities in ringwoodite and bridgmanite at different temperatures for different water contents.

The results of our dislocation recovery experiments indicate that the dislocation motion in ringwoodite is significantly enhanced by the incorporation of water. The dislocation mobility in bridgmanite is therefore higher than that in low-C_{H2O} ringwoodite but lower than that in high-C_{H2O} ringwoodite (Fig. 2C). The Orowan equation suggests that viscosity is inversely proportional to the product of dislocation mobility and density, $\eta \propto 1/(k{\cdot}\rho)$. The dislocation densities in these two minerals are comparable under the same stress conditions (demonstrated in our supplementary experiment detailed in Materials and Methods). Therefore, bridgmanite has a lower viscosity than low-C_{H2O} ringwoodite but a higher viscosity than high-C_{H2O} ringwoodite. The critical C_{H2O} is on the order of thousands of wt ppm (Fig. 2C).

In the context of self-diffusion, the diffusion rates for Si and Mg in bridgmanite (~10^{-19} m^2/s at 1800 K) are higher than the rates for Si and O diffusion in ringwoodite with about 200 wt ppm ($10^{-19.2}$ to $10^{-19.5}$ m^2/s at 1800 K) (*20*, *27*). With a water content exponent of $r = 1.1$, the diffusion rates in water-saturated ($C_{H2O} \approx 3.0$ wt %) and dry ringwoodite ($C_{H2O} <$ 10 wt ppm) are $10^{-17.0}$ and $10^{-20.7}$ m^2/s, respectively. These rates are 2.0 orders of magnitude higher and 1.7 orders of magnitude lower than the rates in bridgmanite, consistent with our dislocation recovery experiments. Thus, our conclusion about ringwoodite viscosity relative to bridgmanite viscosity is also supported by self-diffusion experimental results. Although bridgmanite has been reported to have higher strength than both dry and wet ringwoodite (*29*), these results were based on samples that were deformed under high-stress and low-temperature conditions. Twinning or dynamic recrystallization is known to dominate the creep mechanism under these conditions (*29*). In contrast, Earth's interior (as well as the experimental conditions in this study) has much lower stresses and higher temperatures, and therefore, the thermally activated dislocation climb mechanism should control mineral creep.

A comparison of the values for reciprocal dislocation mobility ($1/k$) for the major minerals in the upper mantle, MTZ, and lower mantle along the adiabatic geotherm (*30*) suggests that incorporation of water significantly reduces $1/k$ in the MTZ (Fig. 3). In addition, although the dislocation mobility in bridgmanite is much smaller than that in olivine at the same temperature (*31*), the lower mantle is approximately 400 K hotter than the upper mantle (*30*), resulting in comparable $1/k$ values after correction for their respective upper and lower mantle geotherms. As a result, if the MTZ is dry, $1/k$ should increase abruptly as the 410-km discontinuity is crossed and then decrease abruptly upon crossing the 660-km discontinuity. In contrast, if the MTZ is hydrous, $1/k$ should behave in the opposite manner, abruptly decreasing across the 410-km discontinuity and increasing across the 660-km discontinuity. As previously mentioned, the postglacial rebound models indicate that the lower mantle's viscosity is at least one order of magnitude higher than the viscosity in the MTZ, and it is comparable to that in the upper mantle (*12*, *13*). Because viscosity is proportional to $1/k$, this mantle viscosity profile suggests that the MTZ stores around 1.5 wt % water (Fig. 3), at least under the regions that have experienced postglacial rebound. If the one-half order of magnitude uncertainty in mantle viscosity is considered, the MTZ must contain at least 1 to 2 wt % water to fit the viscosity profile.

However, note that the lower viscosity in the MTZ compared with the lower mantle is not restricted to postglacial rebound regions. It is a

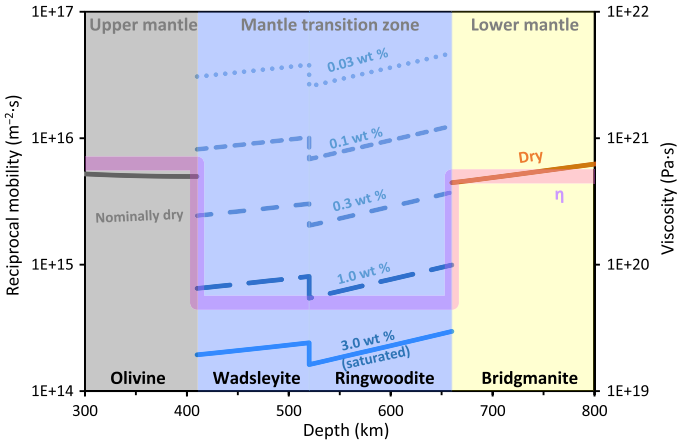

Fig. 3. Reciprocal dislocation mobility (1/*k*) for major minerals in the upper mantle, MTZ, and lower mantle shown in relation to relative viscosity (thick pink line). The relative viscosity (η) is estimated from postglacial rebound data and gravity data (*12*–*14*). The dislocation mobility data for ringwoodite and bridgmanite are from this study, and that for olivine is from Wang (*31*); the dislocation mobility in wadsleyite is assumed to be the same as that for ringwoodite. The activation volume for all minerals is assumed to be 2.6 cm^3/mol (*31*).

global feature based on gravity data (*14*) and a combined analysis of seismic velocity and the geoid (*32*). Also, note that Pearson *et al.* (*3*) found the hydrous ringwoodite inclusion in Brazil, a region that did not experience postglacial rebound. There is no reason to believe that postglacial rebound preferentially occurred above locally hydrous MTZ, and it seems most probable that the water-rich MTZ is a global feature.

The solubility of water in ringwoodite has been found to decrease with increasing temperature (*33*). At MTZ temperatures (*30*), ringwoodite can only store about 0.8 to 1.5 wt % water (*33*). Thus, the MTZ could be nearly water-saturated, especially at the lowest reaches of the MTZ, near depths of 660 km. Partial melts can be produced by excess water, which may account for the observed seismic attenuation in the MTZ (*34*).

Studies of water content in the MTZ based on the electrical conductivity in ringwoodite have estimated that the MTZ contains water at only several thousands wt ppm (*7*–*9*), significantly less than the amounts estimated in this study. Note that the postglacial rebound regions have relatively low conductivity (*6*). If the linear relationship between water content and conductivity (*7*) is considered, high-conductivity regions would exceed the water storage capacity of ringwoodite, which is certainly unrealistic. The exact reasons for these discrepancies are unclear and remain unknown. However, a possibility is that conductivity may not be a sensor for the water content in the MTZ, given the disagreement between the water-rich ringwoodite inclusion (*3*) and the low conductivity beneath Brazil based on magnetotelluric observations (*6*).

MATERIALS AND METHODS

Starting materials

Inclusion-free single crystals of San Carlos olivine ($Mg_{1.8}Fe_{0.2}SiO_4$) with grain sizes of 3 to 6 mm were used as the starting material for ringwoodite synthesis. The crystals were crushed and ground to sub–10-μm powder. For bridgmanite, an orthopyroxene powder ($Mg_{0.89}Fe_{0.11}SiO_3$) synthesized from MgO, FeO, and SiO_2 in a gas-mixing furnace was used. Although natural olivine may contain more impurities than a synthetic starting material, the effect of impurities on dislocation mobility is expected to be small based on the results of recovery experiments on natural and synthetic olivine (*35*).

Synthesis and deformation experiments

Synthesis and deformation experiments were performed using the 5000-ton Kawai-type multianvil press at Okayama University, Japan. The olivine or orthopyroxene powder was wrapped in Re foil and inserted into a Pt capsule. For synthesis of extremely hydrous ringwoodite, the Pt capsule was filled with deionized water and welded in liquid nitrogen. For anhydrous ringwoodite, the capsule was dried in a vacuum furnace and then welded. To simulate moderately hydrous conditions, we welded the capsule without drying. For synthesis of bridgmanite samples, the capsules were welded without any additional treatment.

Each welded capsule was placed in a MgO cylinder inside a $LaCrO_3$ heater with a ZrO_2 thermal insulator. A 5 wt % Cr_2O_3–doped MgO octahedron with a 10-mm edge length was used as the pressure medium (fig. S1A). Eight tungsten carbide cubes with 26-mm edge lengths and 4-mm truncation edge lengths were used to generate high pressures. The assembly was compressed to the target pressure (22 and 25 GPa for ringwoodite and bridgmanite, respectively), heated to 1800 K at a rate of 50 K/min measured by a pair of W97%Re3%-W75%Re25% thermocouples, and kept at the prescribed temperature and pressure for 4 to 5 hours for phase transition and grain growth. The assembly was then further pressurized by about 0.5 GPa within 30 min at 1800 K to produce dislocations in the crystals from uniaxial stresses caused by movement of the Al_2O_3 pistons (fig. S1A). After this, the assembly was quenched to room temperature by switching off the heating power and decompressed to ambient pressure for more than 30 hours. These procedures produced single crystals of ringwoodite that were 400 to 1000 μm in size and aggregates of bridgmanite with grain sizes of 30 to 100 μm. Run product phase identifications were obtained using the Rigaku RAPID II x-ray microdiffractometer at Okayama University.

Dislocation recovery annealing experiments

The bridgmanite aggregates were cut into pieces approximately 400 to 500 μm in size, and each piece was surrounded by CsCl powder, which generated hydrostatic pressure, and wrapped in Re foil for the annealing experiment. For ringwoodite, each single crystal was cut into two pieces. One half was used for transmission electron microscope (TEM) analysis to obtain the initial dislocation density, and the other half was used for recovery annealing. One ringwoodite crystal half for the recovery experiment, together with one or two additional crystals (for water content analysis), was surrounded by CsCl powder, wrapped in Re foil, and inserted into a Pt capsule. The water content in the sample was controlled using a technique similar to that used for the synthesis and deformation experiments: The Pt capsule with anhydrous ringwoodite was dried in a vacuum oven before welding, the capsule with moderately hydrous ringwoodite was welded without any special treatment, and the capsule with extremely hydrous ringwoodite was filled with a small amount of deionized water and Au powder and welded in liquid nitrogen. For both ringwoodite and bridgmanite, the oxygen fugacity (f_{O2}) was controlled by the Re foil. Although Earth's mantle could be more reducing (*36*), the f_{O2} dependence of dislocation mobility in ringwoodite and bridgmanite are expected to be the same because f_{O2} affects their defect chemistry by the same reaction; that is, $3Fe_{Mg}^{x} + \frac{1}{2}O_2 = 2Fe_{Mg}^{\bullet} + V_{Mg}'' + MgO$.

Each capsule with ringwoodite crystals or bridgmanite aggregates was loaded into the multianvil cell assembly with a configuration similar to that used for synthesis and deformation experiments (fig. S1B), compressed to 22 GPa (ringwoodite) or 25 GPa (bridgmanite) at ambient temperature, heated to 1600 to 2200 K, annealed for 0.6 to 24 hours, and then quenched and decompressed to ambient conditions. During annealing, dislocation annihilation occurred through coalescence of

pairs of dislocations with opposite signs, and as a result, dislocation density decreased. X-ray diffraction of the recovered samples confirmed that no phase transitions took place during annealing. In addition, because the ringwoodite samples were single crystals, bridgmanite samples had large grain sizes, and no grain growth occurred during annealing, the effect of grain boundary migration was probably negligible.

Infrared spectroscopy measurements

The water contents in the ringwoodite samples before and after annealing were measured by the high resolution Fourier transform infrared (FT-IR) spectrometer at Okayama University using unpolarized light. Randomly orientated samples were polished on both faces. Two or three spectra for each crystal were obtained on the polished surfaces, and one or two crystals from each run were analyzed. After background and baseline subtraction, the water contents were determined from the FT-IR spectra using the Beer-Lambert law of the form

$$C_{H2O} = \int \frac{3A(\upsilon)M_{H2O}}{\varepsilon_i \tau \rho} d\upsilon \quad (4)$$

where C_{H2O} is the water content in wt ppm, and $A(\nu)$ is the infrared absorption at wave number ν. M_{H2O} is the molar weight of water (18.02 g/mol); ε_i is the absorption coefficient [98,600 liter·mol^{-1}·cm^{-2} for ringwoodite (*37*)]; τ is the sample thickness, which is normalized to 1 cm; and ρ is the density (3900 g/liter). The integration was performed for the wave number range 3740 to 2600 cm^{-1} (*3*). As shown in fig. S2, nominally dry bridgmanite (C_{H2O} < 100 wt ppm) and ringwoodite with different C_{H2O} were obtained, and the C_{H2O} did not change significantly during annealing.

TEM observations

The dislocation densities in the samples before and after dislocation recovery annealing were determined from TEM images. For ringwoodite, electron-transparent samples were obtained using the focused ion beam (FIB) facilities at Ehime University and Hiroshima University. Both pieces (one pristine and one after dislocation recovery annealing) originally cut from the same crystal were polished using diamond powder (0.25 μm) and an alkaline colloidal silica solution before FIB cutting. Two or three FIB foils (approximately 5 × 10 μm^2 foils about 100 nm thick) were obtained from each piece so that the homogeneity of dislocation distribution could be confirmed. Bright-field images (Fig. 1, A and B) were taken at 200-kV acceleration voltage using the field emission gun (FEG) TEM at Ehime University. The visibility of dislocations in the TEM images does not significantly change with two-axis sample tilting. The dominant Burgers vector is a <*uv*0>-type vector, which is consistent with the ½<110> dislocations predicted from numerical modeling (*38*).

For bridgmanite, each sample was polished to a thickness of 30 μm, using diamond powder (0.25 μm). Electron-transparent foils were produced by Ar-ion milling at 3 or 4 kV under a beam angle of 14° at liquid nitrogen temperatures to avoid the amorphization (*39*). Dark-field TEM images, shown in Fig. 1, were taken at the University of Bayreuth, Germany, using an FEG-TEM operated at 200 kV at −168°C using a liquid nitrogen–cooled sample holder. For each sample, different areas of several grains were inspected to confirm the homogeneity of dislocation distribution. Dislocations with diffraction vectors of **g** = 200, 020, or 004 were observed, implying Burgers vectors of **b** = [100], [010], and [001]. The [100] and [010] dislocations are dominant. The [100] dislocations are elongated on the (010) planes (Fig. 1C), whereas long [010] dislocations are curved on the (100) plane. It suggests the (010)[100] and (100)[010] slip systems in bridgmanite, which are different from the (100)[001] slip system reported by deformation experiments (*40*).

Data analysis and uncertainty estimation

Dislocation density can be quantified either by the number of dislocations per unit area or by the total length of dislocations per unit volume. Here, the first method was used because it is difficult to estimate the TEM sample's thickness. In addition, most dislocations in the TEM images are short lines, which would lead to large uncertainties in determining the total dislocation length. The dislocation annihilation rates listed in tables S1 and S2 were calculated from Eq. 1 based on the initial and final dislocation densities (ρ_i and ρ_f, respectively) and the annealing duration. Although the ρ_i in bridgmanite was measured for only a few grains from one sample, it has negligible effect on *k* in Eq. 1 because $\rho_i >> \rho_f$ (table S2).

Farla *et al.* (*35*) have reported that experimentally determined dislocation mobility can be affected by grain boundaries. However, the grain size of the samples used in their study was only several micrometers, similar to the apparent dislocation lengths, whereas the ringwoodite samples synthesized for this study were single crystals. In addition, although our bridgmanite samples were polycrystalline aggregates, the grain sizes were much larger (30 to 100 μm). Therefore, the grain boundary effect in our samples is assumed to be negligible.

We estimated the uncertainty of our data based on three main sources of potential error in this study. First, uncertainty in temperature measurements was present in the annealing experiments, which were around 50 K in 10/4-type multianvil cell assemblies (*41*). With an activation energy of around 330 KJ/mol, temperature uncertainties could cause dislocation mobility to be uncertain by a factor of two. Because the sample and the thermocouple junction were located symmetrically in the furnace in our experiments (fig. S1B), this uncertainty would be much smaller. Second, uncertainty was associated with the FT-IR analysis. This uncertainty can be as large as 50%, but in our experiments, the C_{H2O} values in different crystals from the same run and in the same crystal before and after annealing were almost the same (fig. S2). The maximum change in water content was 43% (0.25 log units) (table S1). Changes of this magnitude had a negligible effect on the linear fits in Fig. 2. Third, there was uncertainty in the dislocation density distribution. As shown in tables S1 and S2, the dislocation densities ρ_i and ρ_f in different TEM specimens cut from the same sample were comparable: All were within a factor of 1.7 except for Run. Rw01. In addition, because the density values were obtained from the number of dislocations per unit area, as previously discussed, any uncertainties associated with estimating the volumes of the TEM specimens were avoided. On the basis of the above estimates, the uncertainties in the dislocation mobilities determined in this study were very small. They appear as the scatter of data points in Fig. 2. This scatter was much smaller than that produced by other experimental techniques used to study mineral rheology in ringwoodite and bridgmanite (*15*, *16*) and almost negligible compared to the contrast in dislocation mobility between bridgmanite and dry or saturated ringwoodite, which differ by a factor of around 100.

Confirmation of similar dislocation densities in ringwoodite and bridgmanite

Viscosity (η) is defined as

$$\eta = \frac{\sigma}{\dot{\varepsilon}} \quad (5)$$

where σ is the stress and $\dot{\varepsilon}$ is the creep rate.

On the basis of the Orowan equation, $\dot{\varepsilon}$ is proportional to dislocation mobility (k), dislocation density (ρ), and Burgers vector ($\mathbf{b}$). That is

$$\dot{\varepsilon} = \rho \mathbf{b} k \quad (6)$$

We could not obtain η in the mantle directly from k because we lack a ρ value under mantle conditions. However, we could obtain the difference in η between ringwoodite and bridgmanite simply by looking at the difference in k because the ρ in various minerals should be similar when they are subjected to the same stress. This outcome results because ρ is only related to the shear modulus and to Burgers vector as described in the Taylor relation (*42*). This similarity in ρ has also been demonstrated by experimental observations (*43*). To further confirm this relationship, we performed an additional experiment in which ringwoodite and bridgmanite were synthesized and deformed in a single experimental run. Olivine and orthopyroxene powders were wrapped in Re foil separately and placed in one cell assembly, compressed to approximately 23.3 GPa, and annealed at 2000 K for 5.5 hours. The olivine and orthopyroxene were transformed into ringwoodite and bridgmanite, respectively, as confirmed by x-ray diffraction of the run products. This phase transition took place because the phase boundary for ringwoodite/post-spinel is about 0.5 GPa higher than that for ilmenite/bridgmanite (*44*). Any dislocations generated in the starting materials during cold compression should have been eliminated during the phase transformations. Subsequently, the assembly was further compressed by 0.1 GPa in 0.5 hours at 2000 K to create dislocations in the crystals. This procedure should have resulted in the stress on the two capsules being exactly the same. TEM observations on the final run products showed comparable dislocation densities in ringwoodite and bridgmanite grains (2.65 and 1.83/μm^2, respectively) (fig. S3). Note that these densities are lower compared to those listed in tables S1 and S2 because a smaller uniaxial stress was applied in this experiment.

SUPPLEMENTARY MATERIALS

Supplementary material for this article is available at http://advances.sciencemag.org/cgi/content/full/3/6/e1603024/DC1

fig. S1. Cross section through the multianvil cell assemblies used for high-pressure experiments.

fig. S2. FT-IR spectra for ringwoodite and bridgmanite before and after dislocation recovery annealing experiments.

fig. S3. Ringwoodite and bridgmanite synthesized from olivine and orthopyroxene and deformed in the same high *P-T* run at 23.3 GPa, 2000 K.

table S1. Experimental conditions, initial and final dislocation densities, and dislocation annihilation rates for ringwoodite.

table S2. Experimental conditions, initial and final dislocation densities, and dislocation annihilation rates for bridgmanite.

REFERENCES AND NOTES

1. D. Bercovici, S.-i. Karato, Whole-mantle convection and the transition-zone water filter. *Nature* **425**, 39–44 (2003).
2. M. M. Hirschmann, Water, melting, and the deep Earth H_2O cycle. *Annu. Rev. Earth Planet. Sci.* **34**, 629–653 (2006).
3. D. G. Pearson, F. E. Brenker, F. Nestola, J. McNeill, L. Nasdala, M. T. Hutchison, S. Matveev, K. Mather, G. Silversmit, S. Schmitz, B. Vekemans, L. Vincze, Hydrous mantle transition zone indicated by ringwoodite included within diamond. *Nature* **507**, 221–224 (2014).
4. S. P. Kelley, J.-A. Wartho, Rapid kimberlite ascent and the significance of Ar-Ar ages in xenolith phlogopites. *Science* **289**, 609–611 (2000).
5. T. H. Torsvik, K. Burke, B. Steinberger, S. J. Webb, L. D. Ashwal, Diamonds samples by plumes from the core–mantle boundary. *Nature* **466**, 352–355 (2010).
6. A. Kelbert, A. Schultz, G. Egbert, Global electromagnetic induction constraints on transition-zone water content variations. *Nature* **460**, 1003–1006 (2009).
7. T. Yoshino, G. Manthilake, T. Matsuzaki, T. Katsura, Dry mantle transition zone inferred from the conductivity of wadsleyite and ringwoodite. *Nature* **451**, 326–329 (2008).
8. X. G. Huang, Y. S. Xu, S.-i. Karato, Water content in the transition zone from electrical conductivity of wadsleyite and ringwoodite. *Nature* **434**, 746–749 (2005).
9. S.-i. Karato, Water distribution across the mantle transition zone and its implications for global material circulation. *Earth Planet. Sci. Lett.* **301**, 413–423 (2011).
10. B. Schmandt, S. D. Jacobsen, T. W. Becker, Z. Liu, K. G. Dueker, Dehydration melting at the top of the lower mantle. *Science* **344**, 1265–1268 (2014).
11. S.-i. Karato, P. Wu, Rheology of the upper mantle: A synthesis. *Science* **260**, 771–778 (1993).
12. J. X. Mitrovica, A. M. Forte, A new inference of mantle viscosity based upon joint inversion of convection and glacial isostatic adjustment data. *Earth Planet. Sci. Lett.* **225**, 177–189 (2004).
13. W. R. Peltier, Postglacial variations in the level of the sea: Implications for climate dynamics and solid-earth geophysics. *Rev. Geophys.* **36**, 603–689 (1998).
14. G. Soldati, L. Boschi, F. Deschamps, D. Giardini, Inferring radial models of mantle viscosity from gravity (GRACE) data and an evolutionary algorithm. *Phys. Earth Planet. Inter.* **176**, 19–32 (2009).
15. J. Girard, G. Amulele, R. Farla, A. Mohiuddin, S.-i. Karato, Shear deformation of bridgmanite and magnesiowüstite aggregates at lower mantle conditions. *Science* **351**, 144–147 (2016).
16. T. Kawazoe, Y. Nishihara, T. Ohuchi, N. Miyajima, G. Maruyama, Y. Higod, K.-i. Funakoshi, T. Irifune, Creep strength of ringwoodite measured at pressure–temperature conditions of the lower part of mantle transition zone using a deformation–DIA apparatus. *Earth Planet. Sci. Lett.* **454**, 10–19 (2016).
17. P. Cordier, T. Ungár, L. Zsoldos, G. Tichy, Dislocation creep in $MgSiO_3$ perovskite at conditions of the Earth's uppermost lower mantle. *Nature* **428**, 837–840 (2004).
18. J. Trampert, H. J. van Heijst, Global azimuthal anisotropy in the transition zone. *Science* **296**, 1297–1299 (2002).
19. S. W. French, B. A. Romanowicz, Whole-mantle radially anisotropic shear velocity structure from spectral-element waveform tomography. *Geophys. J. Int.* **199**, 1303–1327 (2014).
20. A. Shimojuku, T. Kubo, E. Ohtani, T. Nakamura, R. Okazaki, R. Dohmen, S. Chakraborty, Si and O diffusion in $(Mg,Fe)_2SiO_4$ wadsleyite and ringwoodite and its implications for the rheology of the mantle transition zone. *Earth Planet. Sci. Lett.* **284**, 103–112 (2009).
21. A. K. McNamara, S.-i. Karato, P. E. van Keken, Localization of dislocation creep in the lower mantle: Implications for the origin of seismic anisotropy. *Earth Planet. Sci. Lett.* **191**, 85–99 (2001).
22. J.-P. Montagner, B. L. N. Kennett, How to reconcile body-wave and normal-mode reference earth models. *Geophys. J. Int.* **125**, 229–248 (1996).
23. F. Boioli, P. Carrez, P. Cordier, B. Devincre, M. Marquille, Modeling the creep properties of olivine by 2.5-dimensional dislocation dynamic simulations. *Phys. Rev. B* **92**, 014115 (2015).
24. D. L. Kohlstedt, The role of water in high-temperature rock deformation. *Rev. Mineral. Geochem.* **62**, 377–396 (2006).
25. J. Weertman, Dislocation climb theory of steady-state creep. *Trans. Am. Soc. Metals* **61**, 681–694 (1968).
26. S.-i. Karato, M. Ogawa, High-pressure recovery of olivine: Implications for creep mechanisms and creep activation volume. *Phys. Earth Planet. Inter.* **28**, 102–117 (1982).
27. J. Xu, D. Yamazaki, T. Katsura, X. Wu, P. Remmert, H. Yurimoto, S. Chakraborty, Silicon and magnesium diffusion in a single crystal of $MgSiO_3$ perovskite. *J. Geophys. Res.* **116**, B12205 (2011).
28. C. Holzapfel, D. C. Rubie, D. J. Frost, F. Langenhorst, Fe-Mg interdiffusion in $(Mg,Fe)SiO_3$ perovskite and lower mantle reequilibration. *Science* **309**, 1707–1710 (2005).
29. J. H. Chen, D. J. Weidner, M. T. Vaughan, The strength of $Mg_{0.9}Fe_{0.1}SiO_3$ perovskite at high pressure and temperature. *Nature* **420**, 824–826 (2002).
30. T. Katsura, A. Yoneda, D. Yamazaki, T. Yoshino, E. Ito, Adiabatic temperature profile in the mantle. *Phys. Earth Planet. Inter.* **183**, 212–218 (2010).
31. L. Wang, "Temperature and pressure dependence of [100](010) and [001](010) dislocation mobility in natural olivine," thesis, University of Bayreuth (2014).
32. S. D. King, G. Masters, An inversion for radial viscosity structure using seismic tomography. *Geophys. Res. Lett.* **19**, 1551–1554 (1992).
33. E. Ohtani, H. Mizobata, H. Yurimoto, Stability of dense hydrous magnesium silicate phase in the system Mg_2SiO_4-H_2O and $MgSiO_3$-H_2O at pressures up to 27 GPa. *Phys. Chem. Miner.* **27**, 533–544 (2001).
34. B. Romanowicz, J. J. Durek, Seismological constraints on attenuation in the Earth: A review. *Geophys. Monogr.* **117**, 161–179 (2000).
35. R. J. M. Farla, H. Kokkonen, J. D. Fitz Gerald, A. Barnhoorn, U. H. Faul, I. Jackson, Dislocation recovery in fine-grained polycrystalline olivine. *Phys. Chem. Miner.* **38**, 363–377 (2011).
36. D. J. Frost, C. A. McCammon, The redox state of Earth's mantle. *Annu. Rev. Earth Planet. Sci.* **36**, 389–420 (2008).
37. M. Koch-Müller, D. Rhede, IR absorption coefficients for water in nominally anhydrous high-pressure minerals. *Am. Miner.* **95**, 770–775 (2010).

38. P. Carrez, P. Cordier, D. Mainprice, A. Tommasi, Slip systems and plastic shear anisotropy in Mg_2SiO_4 ringwoodite: Insights from numerical modelling. *Eur. J. Mineral.* **18**, 149–160 (2006).
39. N. Miyajima, T. Yagi, M. Ichihara, Dislocation microstructures of $MgSiO_3$ perovskite at a high pressure and temperature condition. *Phys. Earth Planet. Inter.* **174**, 153–158 (2009).
40. N. Tsujino, Y. Nishihara, D. Yamazaki, Y. Seto, Y. Higo, E. Takahashi, Mantle dynamics inferred from the crystallographic preferred orientation of bridgmanite. *Nature* **539**, 81–84 (2016).
41. M. J. Walker, Y. Thibault, K. Wei, R. W. Luth, Characterizing experimental pressure and temperature conditions in multi-anvil apparatus. *Can. J. Geophys. Res.* **73**, 273–286 (1995).
42. S.-i. Karato, *Deformation of Earth Materials: An Introduction to the Rheology of Solid Earth* (Cambridge Univ. Press, 2008), pp. 75–98.
43. D. L. Kohlstedt, M. S. Weathers, Deformation-induced microstructures, paleopiezometers, and differential stresses in deeply eroded fault zones. *J. Geophys. Res.* **85**, 6269–6285 (1980).
44. E. Ito, E. Takahashi, Postspinel transformations in the system Mg_2SiO_4-Fe_2SiO_4 and some geophysical implications. *J. Geophys. Res.* **94**, 10637–10646 (1989).

Acknowledgments: We acknowledge S. Yamashita for help in FT-IR measurement and J. Ando, T. Yoshino, C. Zhao, F. Xu, L. Xie, and L. Wang for discussions. **Funding:** This work was supported by Japan Society for the Promotion of Science funding to H.F. (no. 25003327) and partially supported by Deutsche Forschungsgemeinschaft (DFG) funding to T.K. (no. KA3434/9-1) and DFG grant no. INST 91/315-1 FUGG. **Author contributions:** H.F. and D.Y. organized the project. H.F. conceived the idea for the experiments with help from D.Y. and T.K. The starting materials were prepared by H.F. and M.S. All high-pressure experiments, FT-IR analysis, and FIB cutting were performed by H.F. The TEM sample preparations and observations of bridgmanite were performed by N.M. and H.F., whereas TEM sample preparations and observations of ringwoodite were performed by H.O., H.F., and T.Y. The manuscript was completed by H.F. with discussions and feedback from all coauthors. **Competing interests:** The authors declare that they have no competing interests. **Data and materials availability:** All data needed to evaluate the conclusions in the paper are present in the paper and/or the Supplementary Materials. Additional data related to this paper may be requested from the authors.

Submitted 1 December 2016
Accepted 10 April 2017
Published 7 June 2017
10.1126/sciadv.1603024

Citation: H. Fei, D. Yamazaki, M. Sakurai, N. Miyajima, H. Ohfuji, T. Katsura, T. Yamamoto, A nearly water-saturated mantle transition zone inferred from mineral viscosity. *Sci. Adv.* **3**, e1603024 (2017).

A nearly water-saturated mantle transition zone inferred from mineral viscosity

Hongzhan Fei, Daisuke Yamazaki, Moe Sakurai, Nobuyoshi Miyajima, Hiroaki Ohfuji, Tomoo Katsura and Takafumi Yamamoto

Sci Adv **3** (6), e1603024.
DOI: 10.1126/sciadv.1603024